Proceedings of ASME TURBO EXPO LAND, SEA & AIR '99
The 44th ASME Gas Turbine and AeroEngine Technical Congress
June 7-10, 1999, Indianapolis, IN, USA

IN SITU DETAILED CHEMISTRY CALCULATIONS IN COMBUSTOR FLOW ANALYSES

S. James, M. S. Anand, M. K. Razdan
Rolls-Royce Allison
P. O. Box 420, Speed Code T-14
Indianapolis, IN 46206
and
S. B. Pope
Sibley School of Mechanical and Aerospace Engineering
Cornell University
Ithaca, NY 14853

ABSTRACT

In the numerical simulation of turbulent reacting flows, the high computational cost of integrating the reaction equations precludes the inclusion of detailed chemistry schemes, therefore reduced reaction mechanisms have been the more popular route for describing combustion chemistry, albeit at the loss of generality. The *in situ* adaptive tabulation scheme (ISAT) has significantly alleviated this problem by facilitating the efficient integration of the reaction equations via a unique combination of direct integration and dynamic creation of a look-up table, thus allowing for the implementation of detailed chemistry schemes in turbulent reacting flow calculations. In the present paper, the probability density function (PDF) method for turbulent combustion modeling is combined with the ISAT in a combustor design system, and calculations of a piloted jet diffusion flame and a low-emissions premixed gas turbine combustor are performed. It is demonstrated that the results are in good agreement with experimental data and computations of practical turbulent reacting flows with detailed chemistry schemes are affordable.

INTRODUCTION

The use of detailed kinetic schemes in combustor flow calculations is crucial for the accurate prediction of emissions, ignition, lean blow-out and other performance characteristics. A priori simplification of the detailed chemistry (typically consisting of hundreds of reactions and tens of species) into reduced chemistry schemes consisting of a few steps and species, while computationally efficient, is inadequate for these predictions. Additionally, these combustor performance characteristics are strongly influenced by turbulence/chemistry interactions and accurate prediction of these interactions is equally important. The probability density function (PDF) method offers several advantages over conventional Reynolds-averaged combustion models for the computations of turbulent reacting flows due to the fact that turbulence/chemistry interactions are described exactly by the PDF and chemical kinetics of arbitrary complexity can be incorporated without modeling assumptions. However, due to the enormous computational expense involved in calculations with detailed chemistry schemes, the majority of studies involving PDF methods employ reduced kinetic schemes (Chen *et al.*, 1989) or other techniques to simplify the chemistry such as the intrinsic low-dimensional manifold (ILDM) technique (Anand *et al.*, 1998; Norris, 1998).

The *in situ* adaptive tabulation scheme (ISAT) (Pope, 1997) has significantly relaxed this restriction and detailed chemistry schemes can be economically implemented in PDF calculations. Typically, calculations with reduced chemistry schemes are performed via look-ups from a precalculated table of the results of integration of the reaction rate equations. However, for detailed chemistry calculations, not only will the size of the table be prohibitively large, but also the structure of the table (*i.e.*, independent variables and table intervals) is too complex to accurately and conveniently represent the chemistry. On the other

hand, the direct integration (DI) of the detailed reaction schemes each time it is needed in the calculations is prohibitively expensive. In the *in situ* tabulation procedure, the table is created as needed during the calculations, so that only the compositional region that is appropriate to the flowfield is dynamically generated, stored and accessed repeatedy. Calculations of a homogeneous turbulent reactor have demonstrated that the ISAT scheme provides a speed-up factor of 1000 compared to DI (Pope, 1997). ISAT has also been implemented in calculations using the joint PDF of velocity-frequency-composition (Saxena and Pope, 1998) with resulting speed-ups around 50. For immediate practical applications, the scalar PDF method in which the PDF of composition is solved in conjunction with conventional finite-volume flow-solvers is advantageous, since these flow solvers are computationally affordable and are well developed and matured for complex geometries.

The present study combines the ISAT scheme with a scalar PDF method in a practical combustor design system. The design system is based on a finite-volume solver, which is a conventional pressure-based low-speed variable-density Navier-Stokes solver with a standard $k-\epsilon$ model. The scalar PDF transport equation is solved by an Eulerian Monte-Carlo method, wherein, the PDF at each node is represented by an ensemble of notional particles. This design system in conjunction with reduced chemical kinetics has been applied to diffusion flame swirl combustors and premixed low-emissions combustors (Hsu *et al.*, 1996, 1997). In the present paper, PDF/ISAT calculations of a jet diffusion flame are compared to detailed experimental data including those for the species compositions. Similar calculations are performed on a premixed low-emissions combustor. The successful application of this method for practical gas turbine concepts, such as a low emissions combustor, demonstrates the capability to make detailed species predictions and to optimize combustor design to meet stringent emissions and performance requirements of current and future gas turbine engines. In the following sections, first we briefly describe the PDF method, followed by a description of the ISAT scheme. The results and discussions are presented next, followed by summary and conclusions.

THE SCALAR PDF METHOD

The governing equation for the transport of the joint probability density function $P(\Psi;\mathbf{x},t)$ of the scalars Φ at position $\mathbf{x}$ and t is (Pope, 1976, 1981, 1985):

$$\frac{\partial}{\partial t}(\langle\rho\rangle P)+\frac{\partial}{\partial x_i}(\langle\rho\rangle U_i P)=\frac{\partial}{\partial\psi_\alpha}\left[\langle\rho\rangle\langle\frac{1}{\rho}\frac{\partial J_i^\alpha}{\partial x_i}|\Psi\rangle P\right]$$

$$-\frac{\partial}{\partial x_i}\left[\langle\rho\rangle\langle u_i''|\Psi\rangle P\right]-\frac{\partial}{\partial\psi_\alpha}\left[\langle\rho\rangle S_\alpha P\right]. \qquad (1)$$

where, t is the time, x_i is the ith component of the position vector, ρ is the density, U_i is the ith component of the velocity vector, ψ_α is the mass fraction of species α. J_i^α is the ith component of the diffusional flux for species α, u_i'' is the ith component of the fluctuating velocity, S_α is the source term of species α, Ψ is the set of scalar variables in composition space and Φ is the set of scalar variables in physical space. The notations, $\langle A\rangle$ and $\langle A|B\rangle$, denote the expected value of A and the conditional expectation of A given B, respectively. In the above equation, the terms on the left hand side are the time rate of change and convection by the mean velocity, respectively, of the PDF and are in a closed form. The first term on the right hand side is the influence of molecular mixing on the transport of the PDF in scalar space. The second term on the right hand side represents the transport of the PDF in physical space due to convection by turbulent velocities. These two terms need to be modeled. The last term, which is the effect of reaction source term on the evolution of the PDF in scalar space, is also closed.

Modeling and Discretization

The transport of the PDF in physical space due to turbulent convection is modeled by the gradient diffusion hypothesis (Pope, 1976):

$$\langle\rho\rangle\langle u_i''|\Psi\rangle P=-\langle\rho\rangle D_T\frac{\partial P}{\partial x_i}, \qquad (2)$$

where, D_T is the turbulent diffusivity. Molecular mixing is modeled by the "interaction by exchange with the mean" (IEM) model:

$$\langle\rho\rangle\langle\frac{1}{\rho}\frac{\partial J_i^\alpha}{\partial x_i}|\Psi\rangle P=\langle\rho\rangle C_\phi\omega(\psi_\alpha-\langle\phi_\alpha\rangle)P. \qquad (3)$$

where, C_ϕ is the mixing model constant and ω is the turbulent frequency, defined as the ratio of the turbulent dissipation rate and the turbulent kinetic energy. Past studies on jet diffusion flames (in particular, Flame L of Masri *et al.*, 1988) have shown that the IEM model fails to sustain the flame. Efforts are in progress to develop advanced models (Masri *et al.*, 1996) to better represent the mixing process. In the present study, it is noted that the IEM model is adequate to sustain the flame and is therefore, adopted in all the simulations. The final modeled form of the PDF transport equation is,

$$\frac{\partial}{\partial t}(\langle\rho\rangle P) + \frac{\partial}{\partial x_i}(\langle\rho\rangle U_i P) = \frac{\partial}{\partial \psi_\alpha}\left[\langle\rho\rangle C_\phi \omega(\psi_\alpha - \langle\phi_\alpha\rangle)P\right] + \frac{\partial}{\partial x_i}(\langle\rho\rangle D_T \frac{\partial P}{\partial x_i}) - \frac{\partial}{\partial \psi_\alpha}\left(\langle\rho\rangle S_\alpha P\right). \quad (4)$$

For obtaining the discretized form of the above equation in the finite-volume context, the volume integrals for convection and diffusion terms are first converted to surface integrals using the Gauss theorem and the PDF in each cell is discretized by a hybrid differencing scheme that varies smoothly from an upwind scheme to a central scheme. The resulting equation is

$$P_i(t+\Delta t_i) = P_i(t) + \sum (C_{iK} + D_{iK})(P_k - P_i) + \Delta t_i \frac{M_i(t)}{M_i(t+\Delta t_i)} \frac{\partial}{\partial \psi_\alpha}\left[C_\phi \omega(\psi_\alpha - \langle\phi_\alpha\rangle)P_i\right] - \Delta t_i \frac{M_i(t)}{M_i(t+\Delta t_i)} \frac{\partial}{\partial \psi_\alpha}\left(\langle\rho\rangle S_\alpha P_i\right), \quad (5)$$

where, the index K denotes the faces of cell i and the index k refers to the cell adjacent to cell i across face K. The terms D_{iK} and C_{iK} are the diffusive and convective coefficients and are evaluated as discussed in Anand *et al.* (1998). M_i is the mass in cell i and Δt_i is the time-step in cell i. Equation (5) is solved by a fractional step method in which the transport in physical space is first implemented followed by molecular mixing and chemical reaction. The PDF in each cell is represented by an ensemble of notional particles, each having identical mass and a set of scalar values. The Favre average value of a scalar in a cell is computed by performing an ensemble average of the scalar value on all the particles in the cell. In the present calculations, each cell has an equal number of particles. A variable time-step algorithm Anand *et al.* (1998) is used to accelerate convergence of the solution.

THE ISAT SCHEME

The objective of the ISAT scheme (Pope, 1997; Saxena and Pope, 1998) is to efficiently integrate the coupled set of reaction rate equations:

$$\frac{d\phi_\alpha(t)}{dt} = S_\alpha\left[\Phi(t)\right], \quad (6)$$

i.e., given the initial condition Φ^0, the reaction rate equation is integrated for a time Δt, to obtain $\Phi(t_0 + \Delta t)$. A table is built as the reactive flow calculation progresses, in such a way that only the accessed region of the composition space is tabulated. Since the accessed region is a small subset of the realizable region, the dynamic creation of the table enables efficient integration of the reaction equations than when the table is created *a priori* and the entire realizable region is tabulated. A table entry consists of a composition Φ^0; the mapping $R(\Phi^0)$; the gradient of the mapping $A(\Phi^0)$; and the specification of the ellipsoid of accuracy (EOA). The gradient of the mapping is used in the linear approximation of the mapping

$$R(\Phi^q) \approx R(\Phi^0) + A(\Phi^0)(\Phi^q - \Phi^0) \quad (7)$$

for a query Φ^q. The EOA is an ellipsoidal region, centered at Φ^0, within which the above linear approximation is accurate. As the calculation progresses, the EOA expands such that the error involved in Eqn. (7) is within a user specified tolerance (ϵ_{sp}). The entries in the table are stored in a binary tree which, given a query composition, Φ^q, can be traversed to obtain a table entry Φ^0, which is close to Φ^q. The essential ingredients in the algorithm are summarized below.

1. Given a query composition Φ^q, the binary tree is traversed until Φ^0 is reached.
2. If Φ^q is within the EOA, then the linear approximation Eqn. (7) is returned. This is a *retrieve* (R).
3. Otherwise, a direct integration is performed to determine the mapping $R(\Phi^q)$, and the error ϵ that would result from using Eqn. (7) is determined.
4. If the error is within the tolerance, then the EOA is grown and $R(\Phi^q)$ is returned. This outcome is *growth* (G).
5. Otherwise a new record is generated based on Φ^q. This outcome is an *addition* (A).

RESULTS AND DISCUSSIONS

The $2-D$ finite-volume solver used in the present calculations is a conventional pressure-based low-speed variable-density Navier-Stokes solver (Karki and Patankar, 1988) with a standard $k-\epsilon$ model. The solver employs a staggered grid, with the scalar quantities located at the centers of the cells and the velocities at the cell boundaries. A power-law differencing scheme is used to discretize the governing equations. The finite-volume solver provides the flux to the PDF module which simulates the transport of the scalars. The density change due to turbulent combustion is computed within the PDF module and supplied to the flow-solver and calculations are performed until convergence is achieved.

In all the cases studied, the PDF solver employs 50 particles per cell and the value of the mixing model constant is 2.0. Calculations are performed using two chemistry mechanisms. Table 1 shows a C_1 mechanism involving 16 species and 41 reactions (Yang and Pope, 1998), where A, n and E are the frequency factor, the pre-exponential exponent and the activation energy, respectively. Table 2 shows a 12-step, 16-species augmented C_2 reduced mechanism (ARM) (Chen and Law, 1998) which is derived from the GRI mechanism (Bowman *et al.*, 1995). The flow configurations studied are a piloted jet diffusion flame and a premixed low-emissions gas turbine combustor.

Piloted Jet Diffusion Flame

The flow configuration considered is the piloted jet diffusion flame configuration (Flame D) (Barlow and Frank, 1998) where the radius of the central jet is 3.6 mm and that of the outer annulus of the pilot is 9.1 mm. The fuel jet (having a mixture fraction (Z) value equal to 1) consists of 25% methane and 75% air by volume and the outer coflow is air ($Z = 0$). The pilot burns a mixture of C_2H_2, H_2, CO_2, N_2 and air, having nominally the same equilibrium composition and enthalpy as CH_4/air. The coflow velocity and temperature are 0.9 m/s and $291K$ respectively. The main jet bulk velocity and temperature are 49.6 m/s and $294K$, respectively. The pilot stream has a velocity of 11.4 m/s and a mixture fraction value of 0.27. Calculations are performed on a rectangular domain with 152 cells in the x-direction and 72 cells in the y-direction. The inlet conditions for the velocity and the scalars are specified from the measurements. Free slip boundary conditions are imposed on the top boundary and zero derivative outflow boundary conditions are imposed at the outflow. Symmetry boundary conditions are imposed at the lower boundary (centerline).

A parametric study on the effect of the ISAT error tolerance on the flowfield indicated that a value of 0.008 is adequate to resolve the reacting field of the jet flame. Another study of the turbulent Schmidt number indicates that a value of 2.0 produced the best predictions. For the $k-\epsilon$ constants, the standard values were used for C_μ (= 0.09) and $C_{\epsilon 2}$ (= 1.92), but for $C_{\epsilon 1}$ the standard value of 1.44 as well as a modified value of 1.6 were used for reasons explained later.

Figure 1 presents the contour plot of the Favre temperature in the flowfield with the C_1 chemistry and $C_{\epsilon 1} = 1.6$. It can be noted that just downstream of the pilot, the reaction zone thickness is decreased due to finite-rate chemistry effects. Further downstream, these effects relax and the reaction zone thickness increases. Radial profiles of the mixture fraction f at $x/d = 7.5, 15$ and 30 are presented in Fig. 2. As expected, computations with the standard values

Table 1. 16-SPECIES 41-STEP MECHANISM.

Reaction − step	*A* $mole, cm^3, sec$	*n*	*E* $cal/mole$
$H + O_2 = OH + O$	1.59E+17	-0.927	16874.
$O + H_2 = OH + H$	3.87E+04	2.70	6262.
$OH + H_2 = H_2O + H$	2.16E+08	1.51	3430.
$OH + OH = O + H_2O$	2.10E+08	1.40	-397.
$H + H + M = H_2 + M$	6.40E+17	-1.0	0.
$H + OH + M = H_2O + M$	8.40E+21	-2.00	0.
$H + O_2 + M = HO_2 + M$	7.00E+17	-0.80	0.
$HO_2 + H = OH + OH$	1.50E+14	0.0	1004.
$HO_2 + H = H_2 + O_2$	2.50E+13	0.0	693.
$HO_2 + O = O_2 + OH$	2.00E+13	0.0	0.
$HO_2 + OH = H_2O + O_2$	6.02E+13	0.0	0.
$H_2O_2 + M = OH + OH + M$	1.00E+17	0.0	45411.
$CO + OH = CO_2 + H$	1.51E7	1.3	-758.
$CO + O + M = CO_2 + M$	3.01E+14	0.0	3011.
$HCO + H = H_2 + CO$	7.23E+13	0.0	0.
$HCO + O = OH + CO$	3.00E+13	0.0	0.
$HCO + OH = H_2O + CO$	1.00E+14	0.0	0.
$HCO + O_2 = HO_2 + CO$	4.20E+12	0.0	0.
$HCO + M = H + CO + M$	1.86E+17	-1.0	16993.
$CH_2O + H = HCO + H_2$	1.26E+08	1.62	2175.
$CH_2O + O = HCO + OH$	3.50E+13	0.0	3513.
$CH_2O + OH = HCO + H_2O$	7.23E+05	2.46	-970.
$CH_2O + O_2 = HCO + HO_2$	1.00E+14	0.0	39914.
$CH_2O + CH_3 = HCO + CH_4$	8.91E-13	7.40	-956.
$CH_2O + M = HCO + H + M$	5.00E+16	0.0	76482.
$CH_3 + O = CH_2O + H$	8.43E+13	0.0	0.
$CH_3 + OH = CH_2O + H_2$	8.00E+12	0.0	0.
$CH_3 + O_2 = CH_3O + O$	4.30E+13	0.0	30808.
$CH_3 + O_2 = CH_2O + OH$	5.20E+13	0.0	34895.
$CH_3 + HO_2 = CH_3O + OH$	2.28E+13	0.0	0.
$CH_3 + HCO = CH_4 + CO$	3.20E+11	0.50	0.
$CH_4(+M) = CH_3 + H(+M)$	6.3E14	0.0	104000.
$CH_4 + H = CH_3 + H_2$	7.80E+06	2.11	7744.
$CH_4 + O = CH_3 + OH$	1.90E+09	1.44	8676.
$CH_4 + O_2 = CH_3 + HO_2$	5.60E+12	0.0	55999.
$CH_4 + OH = CH_3 + H_2O$	1.50E+06	2.13	2438.
$CH_4 + HO_2 = CH_3 + H_2O_2$	4.60E+12	0.0	17997.
$CH_3O + H = CH_2O + H_2$	2.00E+13	0.0	0.
$CH_3O + OH = CH_2O + H_2O$	5.00E+12	0.0	0.
$CH_3O + O2 = CH_2O + HO_2$	4.28E-13	7.60	-3528.
$CH_3O + M = CH_2O + H + M$	1.00E+14	0.0	25096.

Table 2. 16-SPECIES 12-STEP AUGMENTED REDUCED MECHANISM.

$$O_2 + 2CO = 2CO_2$$
$$H + O_2 + CO = OH + CO_2$$
$$H_2 + O_2 + CO = H + OH + CO_2$$
$$HO_2 + CO = OH + CO_2$$
$$O_2 + H_2O_2 + CO = OH + HO_2 + CO_2$$
$$O_2 + 0.50C_2H_2 = H + CO_2$$
$$O_2 + CH_3 + CO + C_2H_4 = CH_4 + CO_2 + CH_2O + 0.50C_2H_2$$
$$O_2 + 2CH_3 = H_2 + CH_4 + CO_2$$
$$O_2 + 2CH_3 + CO = CH_4 + CO_2 + CH_2O$$
$$O_2 + CH_3 + CO = H + CO_2 + CH_2O$$
$$O_2 + CO + C_2H_6 = CH_4 + CO_2 + CH_2O$$
$$H + OH = H_2O$$

of the $k-\epsilon$ constants, produce a higher spread rate. This is a common feature observed in computations of round jets and a modified value of $C_{\epsilon 1} = 1.6$ (Pope, 1978) is recommended for this type of flow as a special case. It can be observed that calculations with the modified value produce the correct spread rate. It is also noted that the ARM calculations (C_2 chemistry) with $C_{\epsilon 1} = 1.6$ accurately predict the mean mixture fraction.

Figure 3 presents the radial profiles of the Favre temperature. Consistent with the results from Fig. 2, results for $C_{\epsilon 1} = 1.44$ show a higher spread rate at all the three axial locations. In contrast, calculations with the modified value for both chemistry mechanisms are in excellent agreement with the data. Similar features are also observed in the radial profiles of the major species. Figure 4 presents the radial profiles of CO_2 mass fraction. Calculations with the modified value of $C_{\epsilon 1}$ are in reasonable agreement with the data at all the three axial locations for both reaction mechanisms. Figure 5 presents the radial profiles of the CO mass fraction. It can be observed that the computation with the C_1 mechanism and $C_{\epsilon 1} = 1.44$ overpredicts the peak value and displays a high spread rate at all the three axial locations. In contrast, the C_1 mechanism calculations with the modified value produce the correct spread rate but significantly overpredict the peak value, and at $x/d = 30$ the computed peak value occurs incorrectly at the centerline. The cause of this inaccuracy may be due to the deficiency of the C_1 mechanism for correctly predicting the flame structure in the fuel-rich zones. Calculations performed with the C_2 chemistry (ARM) ($C_{\epsilon 1} = 1.6$) are in reasonable agreement with the data, which indicates that C_2 chemistry is essential to accurately predict CO emissions. Other sources of error in the computations may be due to the neglected influence of radiation heat loss (which reduces the temperature and the CO level), the mixing model used, and the deficiences in the flow solution (spread rate/turbulent transport).

Figure 6 presents the variance of the mixture fraction at three axial locations. Although the calculations with $C_{\epsilon 1} = 1.6$ produce the correct spread rate, the peak values are not in good agreement with the data at $x/d = 15$ and 30. This may be due to deficiencies in the mixing model and the errors/uncertainties involved in the prescription of the inlet turbulent kinetic energy and the turbulent dissipation profiles. The root mean square (RMS) value of temperature is presented in Fig. 7. As with the other quantities the calculation with $C_{\epsilon 1} = 1.6$ is in excellent agreement with the data in regard to the spread rate. Additionally, the peak values are also in good agreement with the data. In comparison, the calculation with the standard value of $C_{\epsilon 1}$ highly overpredicts the spread rate and at $x/d = 30$, the RMS profile does not even have the qualitative feature of the data. The results from the C_2 mechanism are similar to those from the C_1 mechanism with the modified value of $C_{\epsilon 1}$.

The main differences between the C_1 and the C_2 chemistry can be clearly observed from the expected values of species mass fraction and temperature conditioned on mixture fraction. Figure 8 shows the conditional expectation of temperature versus mixture fraction at three axial locations. It can be observed that all the three computations predict the fuel-lean region quite accurately. The fuel-rich region is poorly predicted in the calculation with the C_1 chemistry mechanism, however, the predictions with the C_2 mechanism is excellent. This feature of the two mechanisms is clearly portrayed in Fig. 9 which shows the conditional expectation of CO mass fraction. The C_1 mechanism highly overpredicts the fuel-rich regime; in contrast, the prediction of the C_2 mechanism is reasonable. These results clearly indicate that accurate prediction of CO emissions can be possible only if C_2 chemistry is used in the computations. The prediction of the FLAME D composition structure has been the subject of various investigations which have been summarized in a recent workshop (Barlow and Chen, 1998). A comparison of the results from PDF calculations presented in the workshop with those from the present calculations indicates that overall the flame structure is better predicted by the PDF/ISAT method with the ARM mechanism and $C_{\epsilon 1} = 1.6$.

Premixed Low-Emissions Gas Turbine Combustor

The PDF method with detailed chemistry is applied to a practical gas turbine combustor to demonstrate the feasibility of making detailed performance and emissions calculations. Further, a premixed combustor is chosen since conventional turbulent combustion models fail to predict premixed combustion behavior, and specialized models need to be used. In contrast, the PDF method is equally applicable to nonpremixed and premixed flames.

A radial swirl premixed combustor (Puri *et al.*, 1995) consists of a radial swirl inlet with fuel injectors, a premixer module and the combustor. The flame is stabilized by a recirculating zone outside of the premixer nozzle induced by the swirl motion of the fluid. Bench tests have been performed on this radial swirl combustor and measurements have been obtained for velocity and temperature in the combustor section. The tests were performed with an air flow rate of 0.0635 Kg/s, and an inflow fuel to air ratio of 0.037. The inflow air was preheated to 373 K. The numerical simulation of the combustor is carried out from the exit of the swirler vane and the fuel injector to the exit of the combustor. The fuel injectors are simulated using 6 discrete fuel injection ports at the inlet and calculations are performed on a 151×31 grid. In the calculations, the ignition heat source is simulated by introducing high temperature combustion products downstream of the premixer nozzle. In order to establish a stable flame, ignition is switched on after a swirl induced recirculating zone is established in the flow calculations and turned off after one subsequent timestep of the calculations. The standard values of the $k-\epsilon$ constants are used in these computations. Calculations indicated that an ISAT error tolerance value of 0.008 results in approximately 18 table entries, which is not adequate for an accurate resolution of the flame structure. Therefore, calculations are performed with a tolerance value of 0.001. The C_1 chemistry mechanism is used to demonstrate the capability of ISAT for making computations of practical gas turbines combustors with detailed mechanisms.

Analysis of the mixture fraction field shows that mixing is complete by the time the flow reaches the exit of the premixer where a nearly uniform fuel distribution is found. The swirling motion of the fluid induces a recirculating region near the centerline, downstream of the premixer. Figures 10 and 11 show the cross-stream profiles of the axial and swirl velocities at $x = 221$ and 297 mm, respectively. Although the axial velocities are in good agreement with data, discrepancies in the prediction of the swirl velocities are observed. This is due to the inability of the $k-\epsilon$ model to correctly simulate recirculating flows (Shih *et al.*, 1996) indicating that improved turbulence models are needed to accurately predict these flows. The temperature contours of Fig. 12 show that the flame front is stabilized outside of the premixer nozzle by the recirculating zone and stands in front of the stagnation point of this zone. Comparison of the predicted temperature with experimental data shows excellent agreement at $x = 221$ mm (Fig. 13a) and at $x = 297$ mm (Fig. 13b). These results indicate that the present methodology is capable of accurately predicting realistic combustor characteristics, including turbulent mixing, flow and flame structure and the flame stabilization location. In contrast, calculations using the eddy breakup model (EBU) fail to even qualitatively predict the behavior of the combustor - the EBU model failed to stabilize the flame outside the premixer and always showed flashback (Hsu *et al.*, 1997). The detailed mechanism implemented in the present calculations allows the evaluation of minor species in the flowfield. Due to the lack of experimental data, the accuracy of the predictions of minor species cannot be verified.

Table 3. REGRESSION STATISTICS.

Geometry	Δt_{ret} *sec*	Δt_{gro} *sec*	Δt_{add} *sec*	$Speed-up$
Diffusion Flame	0.000103	0.012	0.428	117
Premix Combustor	0.000109	0.018	0.784	165

ISAT Performance

The efficiency of the ISAT in the scalar PDF calculations is investigated in this section. Results of the regression analyses of the performance data for the two flow configurations studied here are presented in Table 3, where, Δt_{ret} is the retrieve time, Δt_{gro} is the time for growth of the EOA and Δt_{add} is time for the addition of a new record. The analysis is performed for an ISAT error tolerance of 0.008. It can be observed that for both cases studied here, Δt_{ret} is the lowest and Δt_{add} is the highest. The asymptotic value of the speed-up factor, defined as the ratio of growth to retrieve times, is atleast two orders of magnitude higher for the premix combustor calculations.

Figure 14 shows the evolution of the number of records created versus calls to ISAT. It is observed that for an ISAT error tolerance value of 0.008, approximately, 1400 table entries are created in the jet flame computations. In contrast, for the same tolerance value, only 18 entries are created in the combustor calculations. Decreasing the tolerance to 0.001, increases the table entries to 288. Due to the premixed nature of the combustor, the region downstream of the nozzle has an almost uniform composition, therefore the accessed region of the compositional space is significantly

smaller than that in the jet diffusion flame.

A measure of the cumulative CPU time spent in ISAT for the jet flame calculations can be obtained from Fig. 15 which shows the fraction of time spent in ISAT versus the number of calls. It can be observed that after 10^6 calls, almost 60% of the time is spent in evaluating chemistry. For the premix combustor, approximately, 80% of the time is spent in chemistry. The evolution of the speed-up factor which is the ratio of the time taken to perform the calculations using DI to that using ISAT, is presented in Fig. 16. It can be observed that after the initial transients, the curve flattens to a value of approximately 117. Values close to 200 have been observed in previous joint velocity-scalar PDF calculations. Although the storage requirement for the coarse tolerance level used in the jet flame calculations is not significant, it can become a serious issue when lower tolerance levels are required. Correspondingly, the CPU time will also increase for simulations with a lower tolerance value.

SUMMARY AND CONCLUSIONS

The present paper demonstrates the application of detailed chemical kinetics in scalar PDF computations of a jet diffusion flame and a practical premixed low-emissions gas turbine combustor. The jet diffusion flame calculations with a modified value of one of the $k-\epsilon$ constants ($C_{\epsilon 1} = 1.6$) and C_1 chemistry, produce good agreement of the major species mass fractions and temperatures with the experimental data. For accurate prediction of CO emissions, it has been shown that C_2 chemistry schemes have to be used. Computations of the premixed swirl combustor also indicate good agreement with experimental data for temperatures and velocities. The behavior of the combustor including the location and extent of the flame are well predicted.

Performance analyses of ISAT show that speed-up factors of 117 and 165 are achieved in the computations for the jet diffusion flame and the premix combustor, respectively. The cumulative fraction of time spent in evaluating chemistry is 0.6 and 0.8 for the jet diffusion flame and the premixed combustor, respectively. The number of records created in the premixed combustor calculations is significantly lower than the jet calculations, which indicates that the accessed region of the scalar space for the premix flame is significantly smaller than that for the diffusion flame. These calculations indicate that using ISAT, details of the major and minor species in practical combustors can be obtained at an affordable cost. Consideration of minor species in the detailed mechanism allows the prediction of emissions. Accurate prediction of emissions for practical combustors is the subject of ongoing investigations.

ACKNOWLEDGEMENTS

This work is sponsored in part by the U.S. Department of Energy, Federal Energy Technology Center under co-operative agreement # DE-FC21-92-MC29061 through the Advance Gas Turbine Systems Research (AGTSR) with Dr. Daniel Fant as the program manager.

References

Anand, M. S., James, S., and Razdan, M. K. (1998). A scalar PDF combustion model for the National Combustion Code. AIAA Paper AIAA-98-3856.

Barlow, R. S. and Chen, J. Y. (1998). Third international workshop on measurement and computation for turbulent nonpremixed flames. *http://www.ca.sandia.gov/ tdf/ 3rdWorkshop/ Boulder.html* .

Barlow, R. S. and Frank, J. H. (1998). Effects of turbulence on species mass fractions in methane/air jet flames. In *Proceedings of 27rd Symp. (Int.) on Combustion.* The Combustion Institute, Pittsburgh, PA.

Bowman, C. T., Hanson, R. K., Davidson, D. F., Gardiner Jr, W. C., Lissianski, V., Smith, G. P., Golden, D. M., Frenklach, M., and Goldenberg, M. (1995). *http:// www.me.berkeley.edu/gri_mech* .

Chen, J. Y. and Law, C. K. (1998). Poster. In *Proceedings of 27rd Symp. (Int.) on Combustion.* The Combustion Institute, Pittsburgh, PA.

Chen, J. Y., Kollmann, W., and Dibble, R. W. (1989). PDF modeling of turbulent nonpremixed methane jet flames. *Combust. Sci. and Tech.* **64**, 315–346.

Hsu, A. T., Anand, M. S., and Razdan, M. K. (1996). An assessment of PDF versus finite-volume methods for turbulent reacting flow calculations. AIAA Paper AIAA-96-0523.

Hsu, A. T., Anand, M. S., and Razdan, M. K. (1997). Calculation of a premixed swirl combustor using the PDF method. In *42nd ASME Gas Turbine and Aero Engines Congress, Orlando, Florida.*

Karki, K. C. and Patankar, S. V. (1988). Calculation procedure for viscous incompressible flows in complex geometries. *Numerical Heat Transfer* **14**.

Masri, A. R., Bilger, R. W., and Dibble, R. W. (1988). Turbulent nonpremixed flames of methane near extinction: Mean structure from Raman measurements. *Combust. Flame* **71**, 245–266.

Masri, A. R., Subramanium, S., and Pope, S. B. (1996). A mixing model to improve the PDF simulations of turbulent diffusion flames. In *Proceedings of 26rd Symp. (Int.) on Combustion.* The Combustion Institute, Pittsburgh, PA.

Norris, A. T. (1998). Automatic simplification of full chemi-

cal mechanisms: Implementation in National Combustion Code. AIAA Paper AIAA-98-3987.

Pope, S. B. (1976). The probability approach to modeling of turbulent reacting flows. *Combust. Flame* **27**, 299–312.

Pope, S. B. (1978). An explanation of the turbulent round-jet/plane-jet anomaly. *AIAA J.* **16**, 279–281.

Pope, S. B. (1981). A Monte-Carlo method for the PDF equation of turbulent reactive flow. *Combustion Science and Technology* **25**.

Pope, S. B. (1985). PDF methods for turbulent reacting flows. *Prog. Energy Combust. Sci.* **11**, 119–192.

Pope, S. B. (1997). Computationally efficient implementation of combustion chemistry using in situ adaptive tabulation. *Combust. Theory. Modeling* **1**, 41–63.

Puri, R., Stansel, D. M., Smith, D. A., and Razdan, M. K. (1995). Dry ultra-low NOx green thumb combustor for Allison's 501-K series industrial engines. ASME Paper 95-GT-406.

Saxena, V. and Pope, S. B. (1998). PDF simulations of turbulent combustion incorporating detailed chemistry. *Combust. Flame, to be published* .

Shih, T. H., Zhu, J., and Lumley, J. L. (1996). Calculation of wall-bounded complex flows and free shear flows. *International Journal for Numerical Methods in Fluids* **23**, 1–12.

Yang, B. and Pope, S. B. (1998). An investigation of the accuracy of manifold methods and splitting schemes in the computational implementation of combustion chemistry. *Combust. Flame* **112**, 16–32.

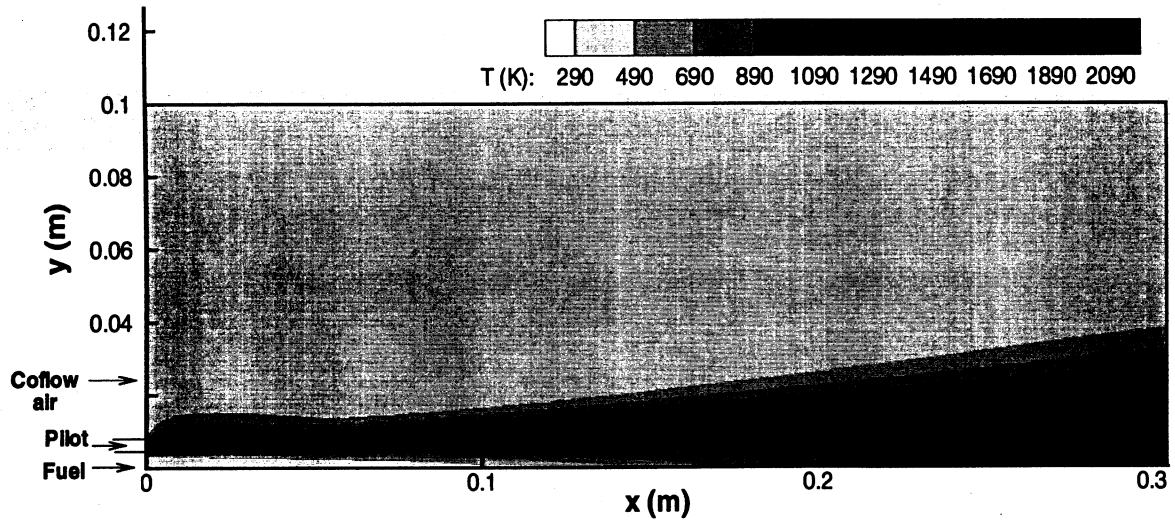

Figure 1. CONTOURS OF THE FAVRE MEAN TEMPERATURE IN THE FLOWFIELD.

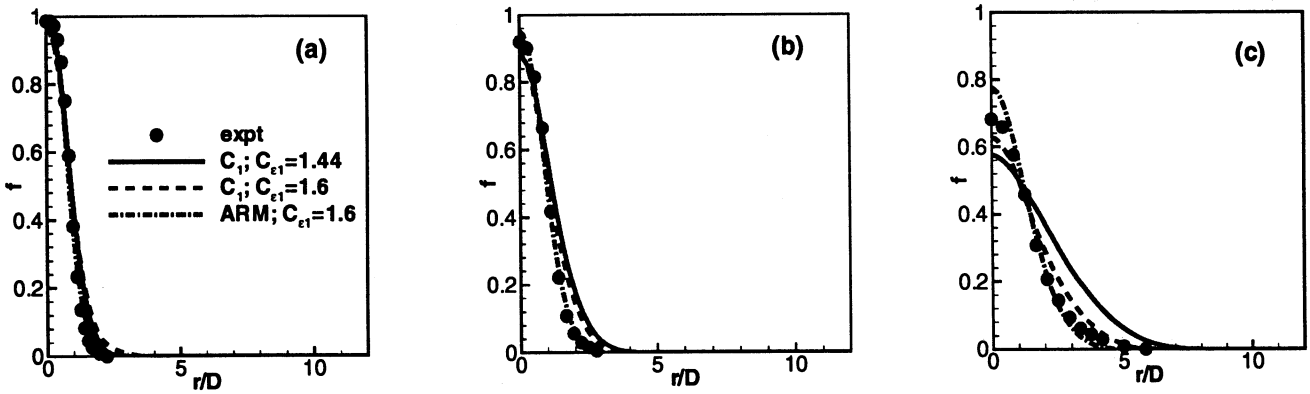

Figure 2. RADIAL PROFILES OF MEAN MIXTURE FRACTION FROM CALCULATIONS WITH THE C_1 AND THE ARM MECHANISM. (a) $X/D = 7.5$, (b) $X/D = 15$ AND (c) $X/D = 30$.

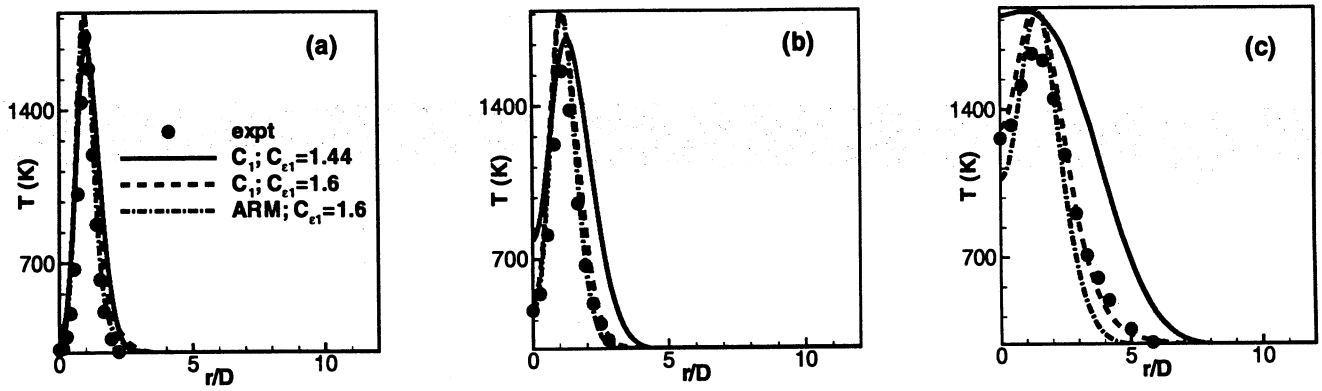

Figure 3. RADIAL PROFILES OF MEAN TEMPERATURE. (a) $X/D = 7.5$, (b)$X/D = 15$ AND (c) $X/D = 30$.

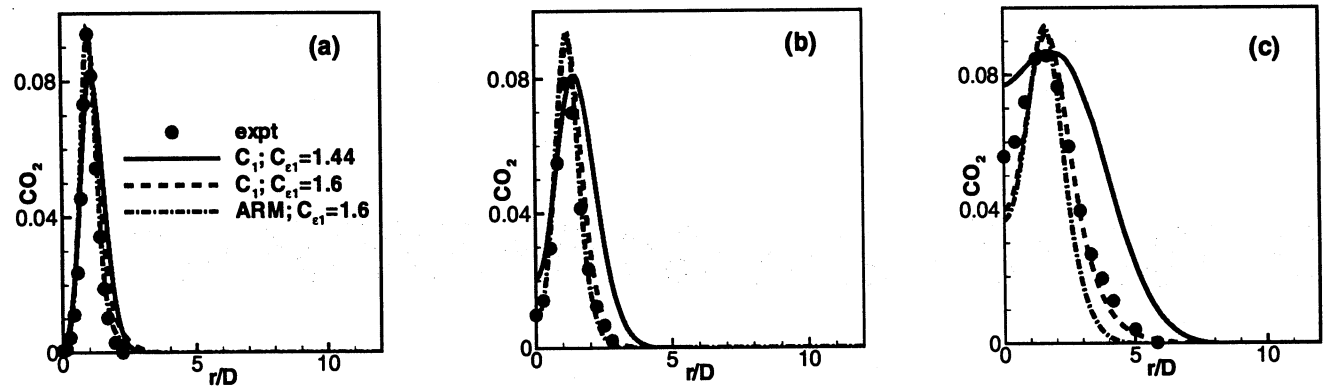

Figure 4. RADIAL PROFILES OF MEAN CO_2 MASS FRACTION. (a) $X/D = 7.5$, (b) $X/D = 15$ AND (c) $X/D = 30$.

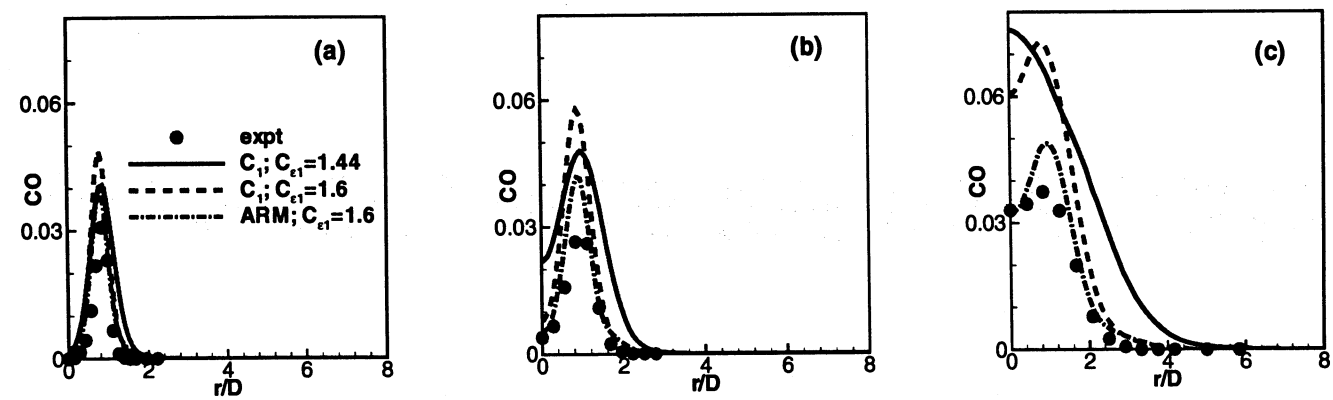

Figure 5. RADIAL PROFILES OF MEAN CO MASS FRACTION. (a) $X/D = 7.5$, (b) $X/D = 15$ AND (c) $X/D = 30$.

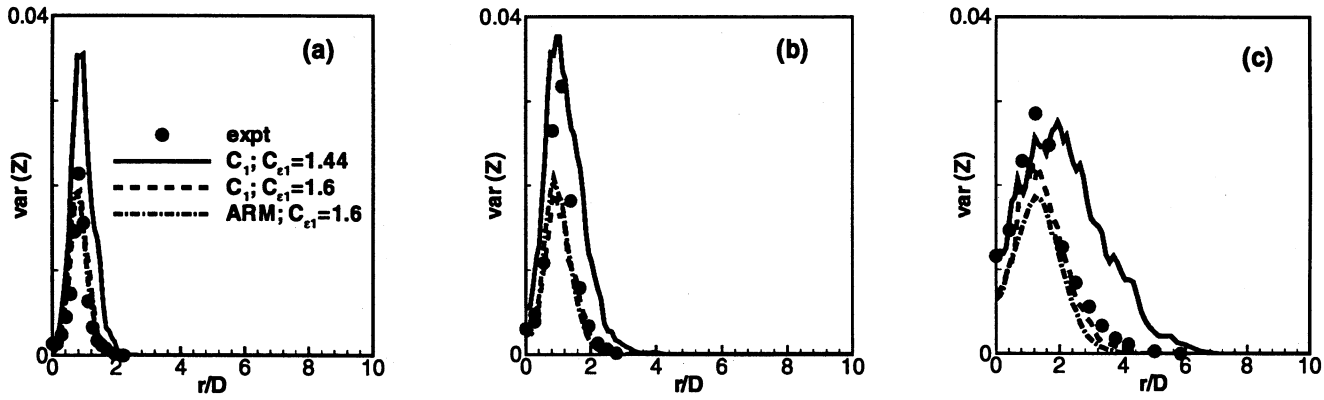

Figure 6. RADIAL PROFILES OF THE VARIANCE OF MIXTURE FRACTION. (a) $X/D = 7.5$, (b) $X/D = 15$ AND (c) $X/D = 30$.

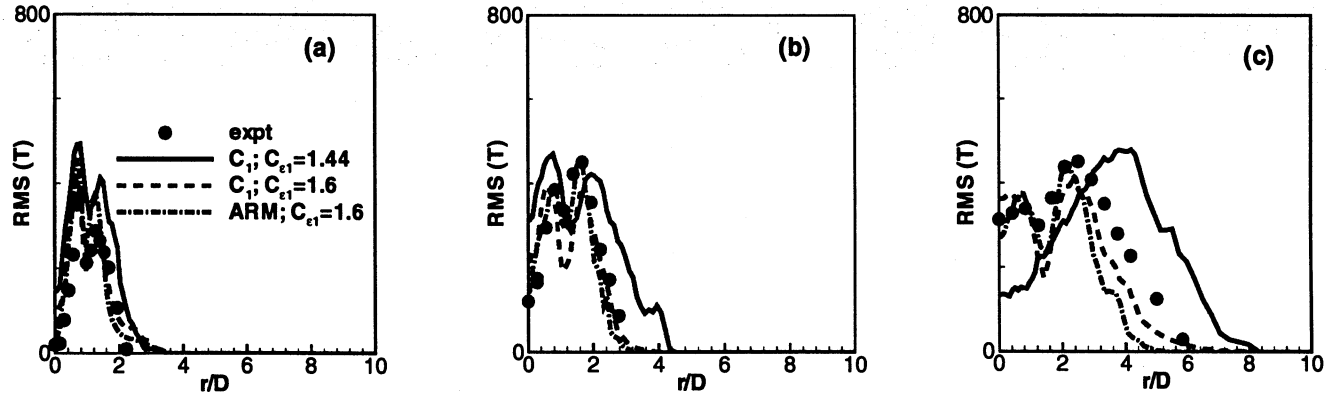

Figure 7. RADIAL PROFILES OF THE RMS OF T. (a) $X/D = 7.5$, (b) $X/D = 15$ AND (c) $X/D = 30$.

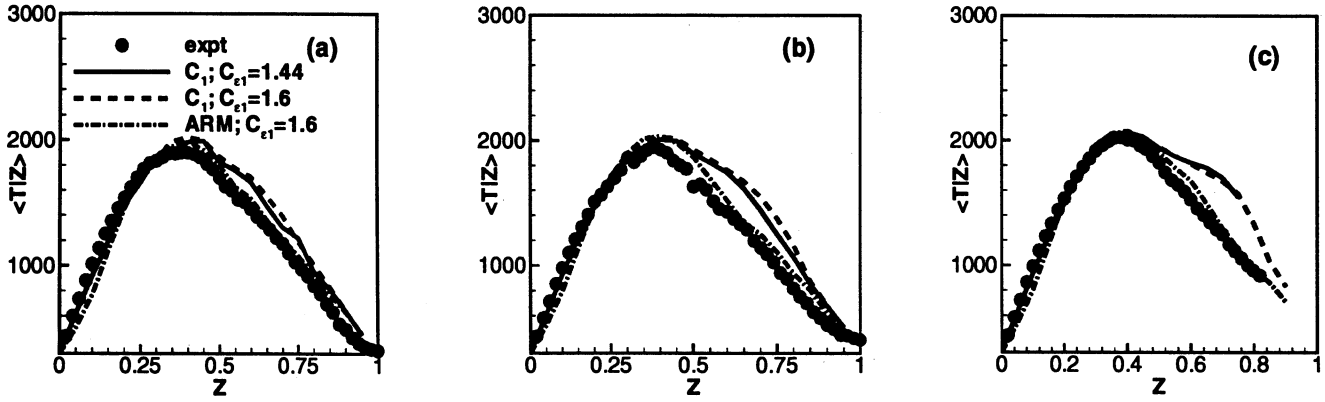

Figure 8. CONDITIONAL EXPECTATION OF T. (a) $X/D = 7.5$, (b) $X/D = 15$ AND (c) $X/D = 30$.

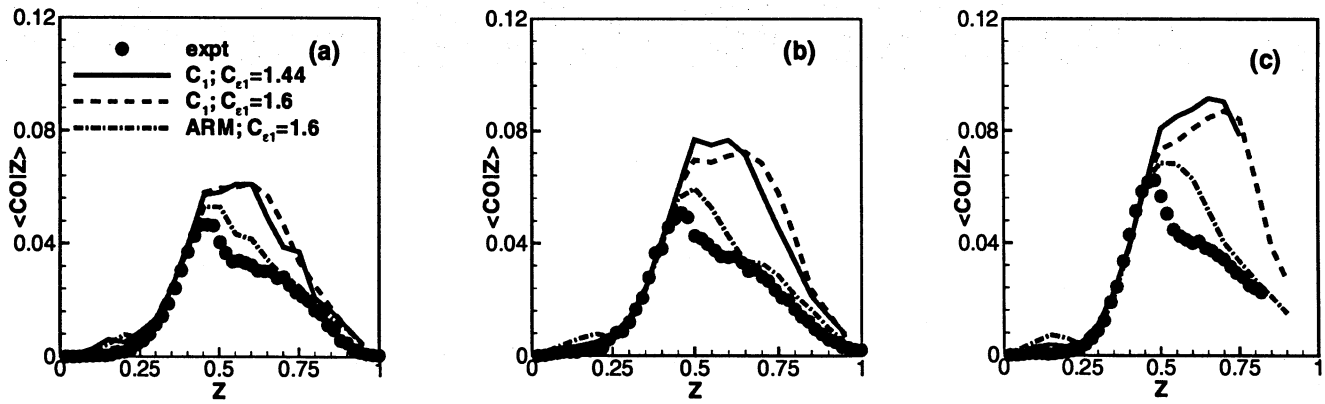

Figure 9. CONDITIONAL EXPECTATION OF CO. (a) $X/D = 7.5$, (b) $X/D = 15$ AND (c) $X/D = 30$.

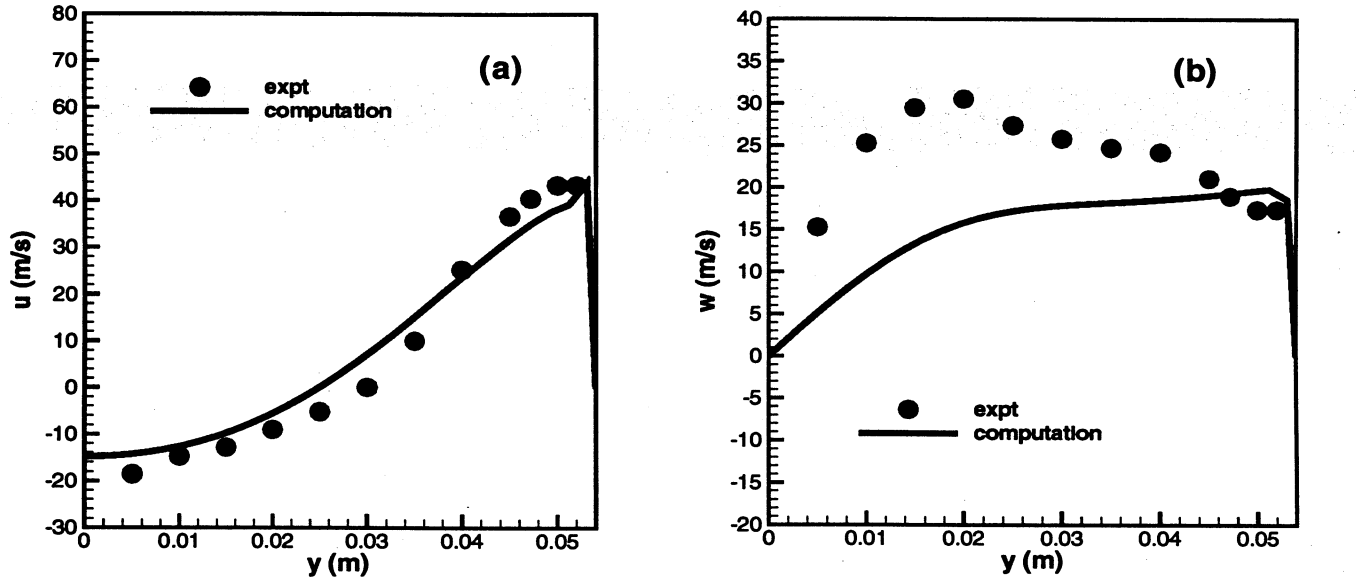

Figure 10. CROSS-STREAM PROFILES OF (a) MEAN AXIAL VELOCITY AND (b) MEAN SWIRL VELOCITY AT $X = 0.221$ m.

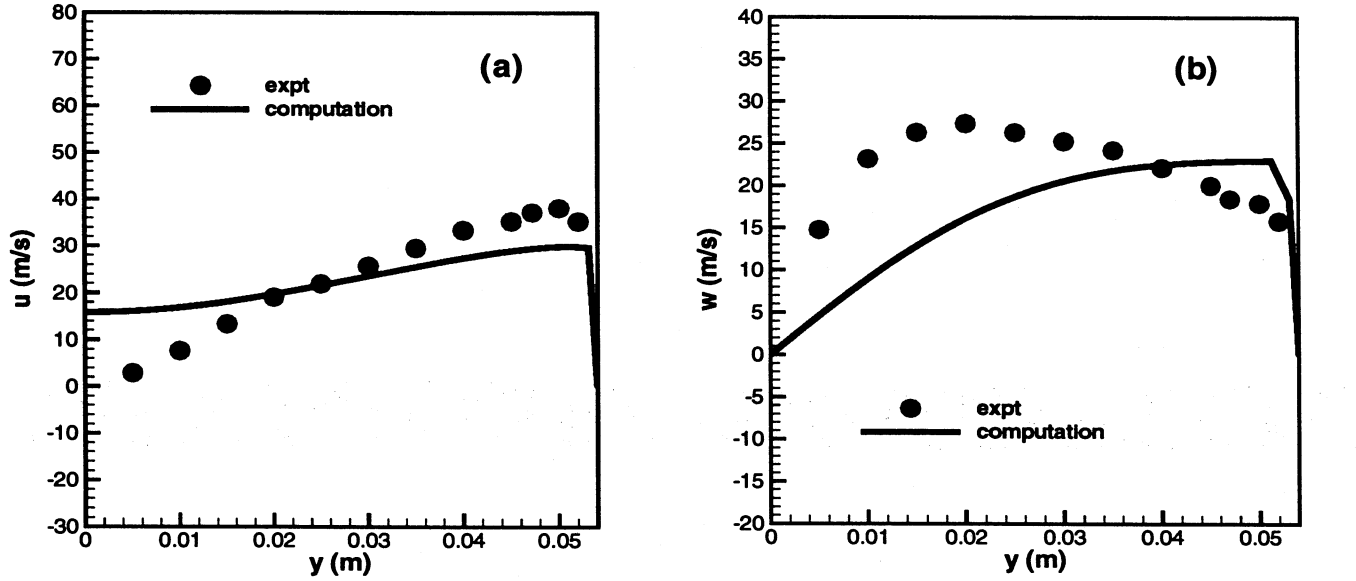

Figure 11. CROSS-STREAM PROFILES OF (a) MEAN AXIAL VELOCITY AND (b) MEAN SWIRL VELOCITY AT $X = 0.297$ m.

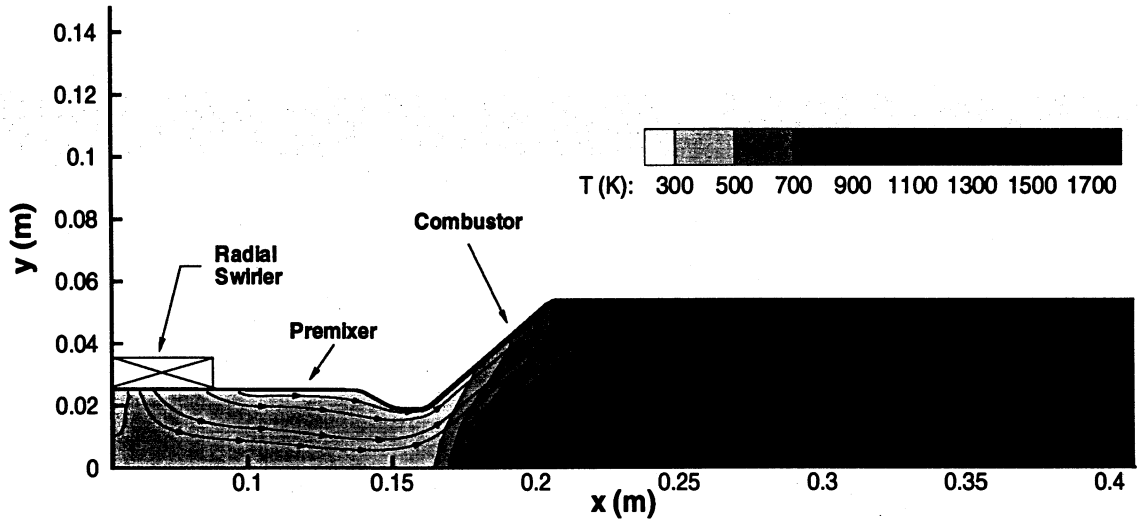

Figure 12. CONTOURS OF THE FAVRE MEAN TEMPERATURE AND SAMPLE STREAMTRACES IN THE PREMIX COMBUSTOR.

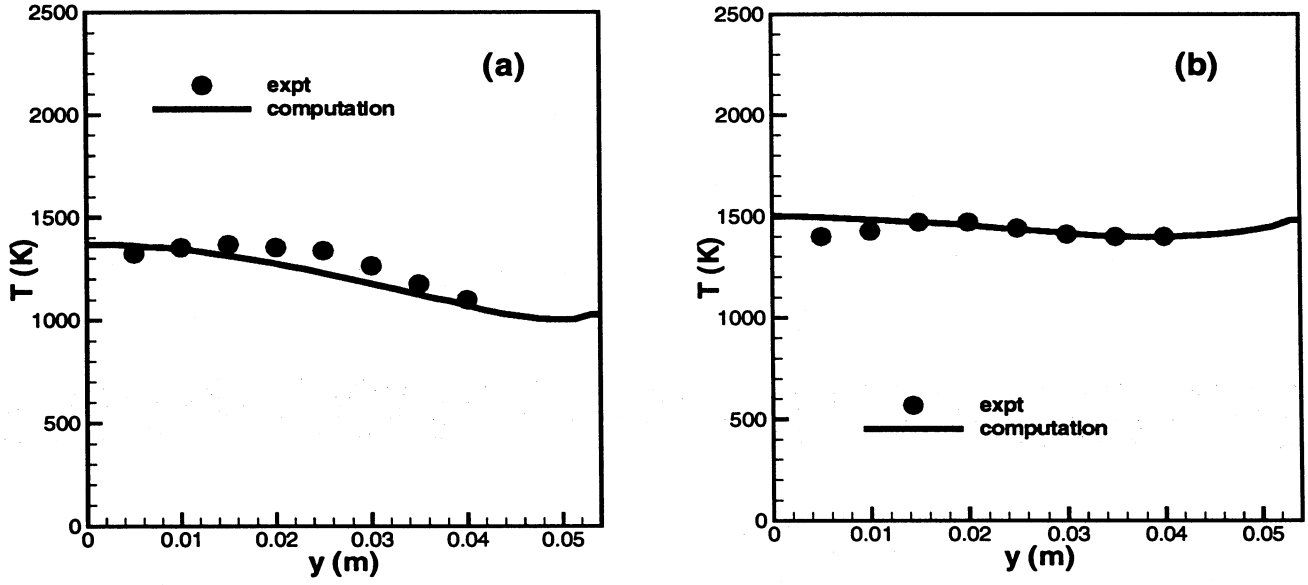

Figure 13. CROSS-STREAM PROFILES OF MEAN TEMPERATURE AT (a) $X = 0.221$ m and (b) $X = 0.297$ m.

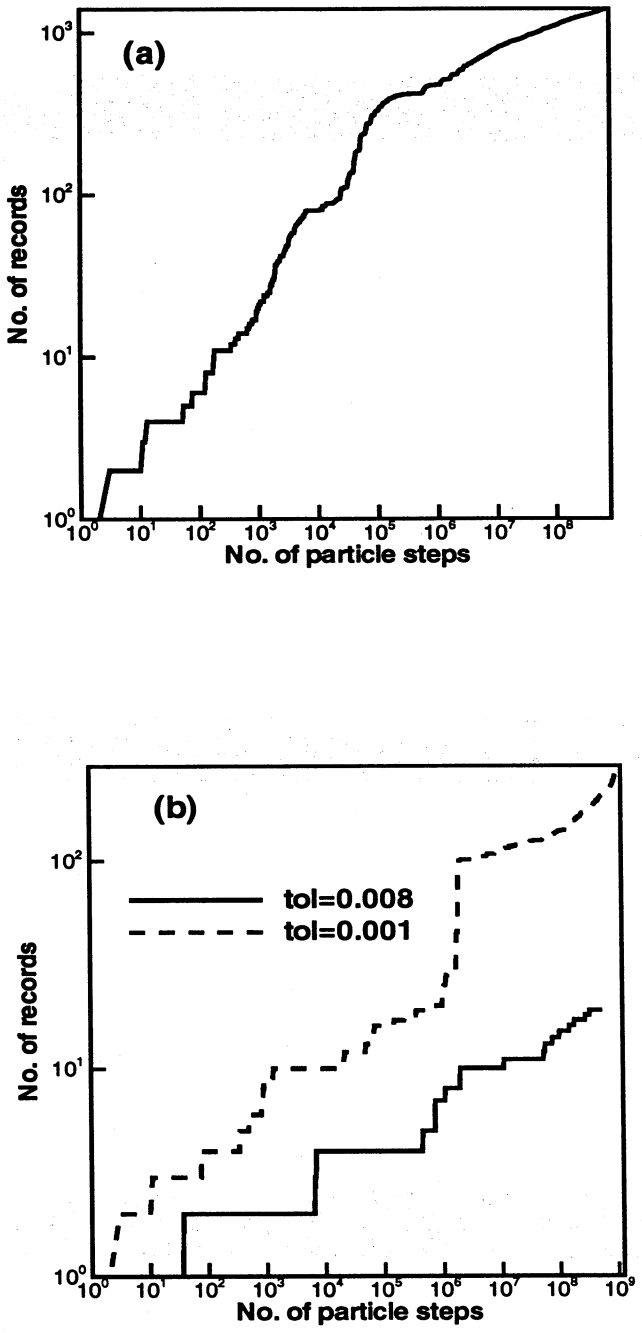

Figure 14. EVOLUTION OF THE NUMBER OF RECORDS. (a) JET DIFFUSION FLAME. (b) PREMIX COMBUSTOR.

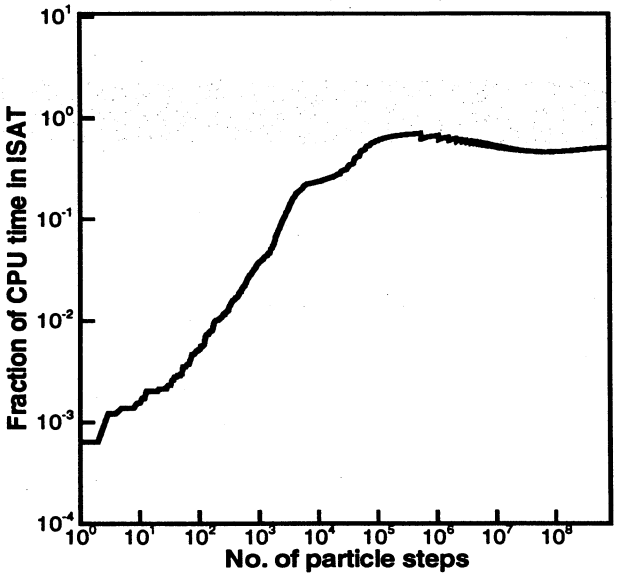

Figure 15. FRACTION OF THE CPU TIME SPENT IN ISAT FOR THE JET DIFFUSION FLAME.

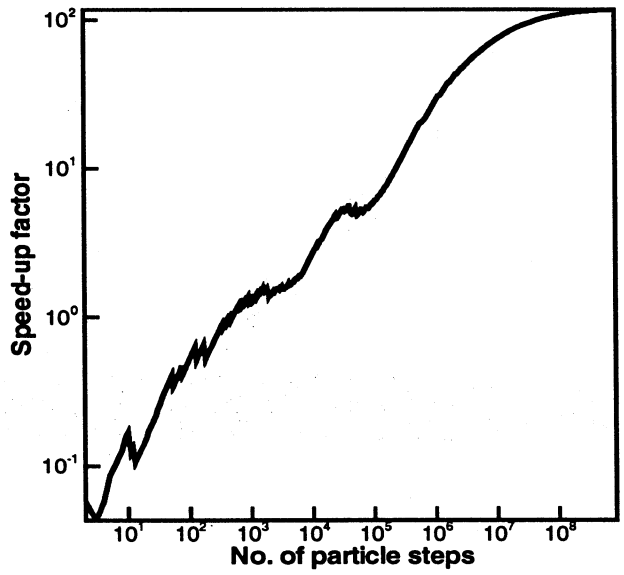

Figure 16. SPEED-UP FACTOR OF ISAT OVER DI FOR THE JET DIFFUSION FLAME.